JOURNAL OF AIRCRAFT
Vol. 48, No. 3, May–June 2011

Engineering Notes

Performance of Coflow Jet Airfoils with Conformal Slot Geometries

Jun-Mei Zhang,* Tat Loon Chng,† and Her Mann Tsai‡
National University of Singapore,
Singapore 119260, Republic of Singapore

DOI: 10.2514/1.C031145

Nomenclature

b	=	airfoil span, m
C_p	=	static pressure coefficient, $(p_s - p_\infty)/(0.5\rho_\infty V_\infty^2)$
C_μ	=	jet momentum coefficient, $\dot{m}_j V_j/(0.5\rho_\infty V_\infty^2 S)$
c	=	airfoil chord, m
Ma	=	freestream Mach number
$\dot{m}_j$	=	jet mass flow rate, kg/s
p_s	=	airfoil static pressure, Pa
p_∞	=	freestream static pressure, Pa
Re	=	Reynolds number, $\rho_\infty V_\infty c/\mu$
S	=	projected wing area, $b \times c$, m^2
V_j	=	jet injection bulk velocity, m/s
V_∞	=	freestream velocity, m/s
X	=	distance from the airfoil leading edge, m
α	=	angle of attack, °
ρ_∞	=	freestream density, kg/m^3
μ	=	freestream dynamic viscosity, kg/m · s

I. Introduction

ACTIVE flow control via fluid injection and suction, such as circulation control (CC) [1] and pulsed flow control [2,3], has been one of the most promising methodologies for augmenting aircraft performance. Amongst others, the coflow jet (CFJ) airfoil first proposed by Zha et al. [4–6], Zha and Paxton [7], and Zha and Gao [8] has gained considerable attention. This concept involves the creation of two suitably located spanwise slots along an airfoil from which fluid can be tangentially expelled and ingested. A suggested viable configuration is to have these slots on the airfoil upper surface, one at the leading edge which injects fluid and the other at the trailing edge for fluid suction. The strong turbulence diffusion and mixing between the main flow (freestream) and the auxiliary flow (injection and suction) is believed to enhance lateral transport of energy from the latter to the main flow which suppresses flow separation and in turn produces an increase in lift and stall margin [4,9]. A net thrust can even be achieved when the momentum coefficients of the injection and suction are sufficiently high. The ingenuity of this approach is that the fluid sucked-in can be simultaneously used as the injection source. In this way, rather than using two separate sources for active flow control, only one source is required and the thrust penalty of dumping the injected fluid is avoided.

One drawback of this technique is related to the geometry of the spanwise slots. A previous slot design aimed at realizing tangential flow has resulted in a modified airfoil (as shown in Fig. 1a), which produces poorer performance than the unmodified airfoil in the absence of blowing and suction [9,10]. To overcome this drawback, a novel conformal design of the injection and suction slots shown in Fig. 1b has been proposed by our group [11].

In this note, the performance of a CFJ airfoil based on this conformal design is evaluated. In particular, the effect of blowing from either the upper or lower surface is examined. The latter is inspired by the counterfluid injection approach first proposed by Wake et al. [12], which has been found to surpass conventional upper surface blowing methods. Reasons for its superior performance include a "virtual shaping effect" [13], enhancement of turbulent mixing, a prolonged shear layer development path, and the natural flow acceleration due to the favorable pressure gradient over the upper surface at high angles of attack (AOA). Apart from combined injection and suction, the performance of injection and suction when conducted individually, [i.e., streamwise blowing (SB), counter-streamwise blowing (CB) and suction (S))] is also investigated.

II. Experimental and Numerical Simulation Methodologies

A. Experimental Method

A Clark Y airfoil is selected as the baseline model because of its simple yet robust design. This baseline airfoil is modified to have conformal injection and suction slots as shown in Fig. 1b. The model is fabricated using a rapid prototyping technique. Several steel rods and vertical support pillars are included within the design so as to maintain the structural integrity of the internal ducts. The test model has a chord c of 210 mm and a span b of 390 mm. The injection slot on the lower and upper surfaces is located at $X/c = 0.032$ and $X/c = 0.036$ separately with a height of $0.005c$ and $0.00419c$, respectively. The suction slot is located at $X/c = 0.87$ with a height of $0.01c$ to prevent flow choking [4,7]. Two small steel tubings with a diameter of 1 mm are inserted on the lower and upper surfaces, respectively, along the airfoil span at $X/c = 0.01$ to trip the flow and ensure consistency with the computations and real life applications. Since both injection slots share the same internal duct, depending on whether counterstreamwise or streamwise injection is conducted, the slot not in use is sealed using silicone to prevent leakage. Likewise, since the airfoil geometry is conformal, both injection slots are sealed to "replicate" the baseline airfoil.

A total of 38 static pressure taps are located along the midspan of the airfoil, of which 21 are located on the upper surface and 17 on the lower surface. Besides pressure measurements, lift and drag measurements are conducted by suspending an unmodified Clark Y airfoil on an ATI Gamma force balance with 6 degrees of freedom. These corresponding force measurements for the modified airfoils with jet injection and/or suction are not reported, as they are insufficiently reliable due to significant interference of the internal ducts with the load measurements. Detailed information on the test rig can be found in [9,11].

Tabulated in Table 1 are the test cases for the wind-tunnel pressure measurements. The definition of the momentum coefficient is:

$$C_\mu = \dot{m}_j V_j/(0.5\rho_\infty V_\infty^2 S) \tag{1}$$

where $\dot{m}_j$ is the jet mass flow rate, V_j the bulk velocity of the jet, S the projected wing area, and ρ_∞, V_∞ are the freestream density and velocity, respectively.

Presented as Paper 2008-335 at the 46th AIAA Aerospace Sciences Meeting and Exhibit, Reno, NV, 7–10 January 2008; received 16 June 2010; revision received 7 January 2011; accepted for publication 19 January 2011.

*Research Fellow, Department of Mechanical Engineering, 10 Kent Ridge Crescent.
†Associate Scientist, Temasek Laboratories, 1 Engineering Drive 2.
‡Principle Research Scientist, Temasek Laboratories, 1 Engineering Drive 2.

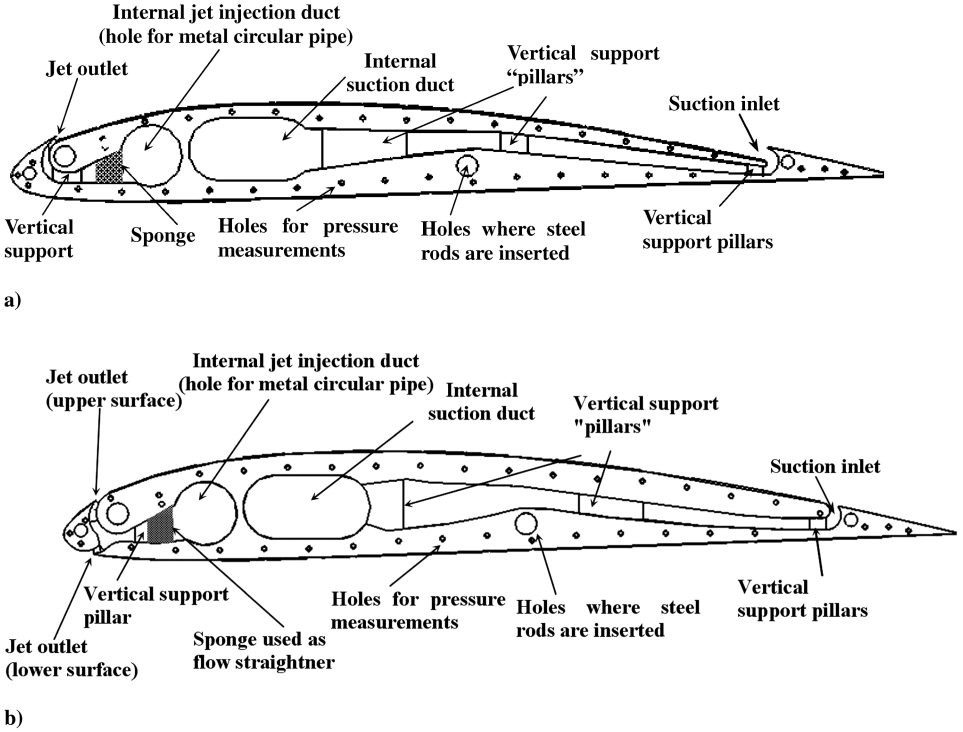

Fig. 1 A cross-sectional schematic of the modified airfoil used for the wind-tunnel experiments with: a) nonconformal and b) conformal design of injection and suction slots.

B. Numerical Simulation Approach

Computational investigations are performed using FLUENT™. Since considerable effort has been devoted to achieving spanwise uniformity of the flow in the experiments, two-dimensional (2-D) simulations are performed. Reynolds-averaged Navier–Stokes (RANS) equations which have proven to be an efficient and reliable tool for similar flow problems [9,12] are solved.

The shear-stress transport (SST) k-ω turbulent model is used. A second-order upwind scheme is applied for discretization. A normalized residual of 10^{-4} is set as the convergence criterion, which determines when the iterations are terminated. To monitor the convergence of the solution, the changes of lift and drag coefficients with the advancement of iterations are plotted and checked. Shown in Figs. 2a–2f are meshes for the baseline Clark Y and modified airfoils for the different combinations of injection and suction. These grids consist of a total of 54636, 70096, 75584, 68472, 78484, and 67432 cells, respectively. To adequately resolve the regions affected by viscosity, fine near-wall meshes spacing on the order of $y^+ = 1$ are used. Grid independency is checked for the baseline and SB-S cases.

The computational domain for all the airfoils encompasses a half-circle of radius $15c$ upstream of the trailing edge of the airfoils and a rectangular region beyond the trailing edge measuring $25c$ in width and $30c$ in height. The flow within the internal ducts is not included in the simulations as they have been found to have an insignificant effect on the flow around the airfoil [6]. As far as possible, boundary conditions, particularly those in Table 1, are chosen to match those of the experiments.

III. Results and Discussion

A. Comparison of Pressure Coefficient Distributions

Figure 3 shows the pressure coefficient C_p distributions for the baseline and modified airfoils (SB, SB-S, and S configurations) obtained from numerical simulations and wind-tunnel tests. For the baseline airfoil, the computational results are in good agreement with the experiments for all AOAs from 0 to 16°, except at three points ($X/c = 0.05$, 0.10, and 0.15) located just downstream of the injection slot on the upper surface. The discrepancy at these points may be due to the unevenness in the airfoil surface in the experiments created as a result of sealing up the injection slot with silicone. At AOA of 16°, both computational fluid dynamics (CFD) and experimental results reveal the occurrence of flow separation as indicated by flat sections of the C_p curve near the trailing edge (as seen in Fig. 3d). However, flow separation predicted by simulation results at AOA = 20° occurs earlier than in the experiments. This may be attributable to the weakness of the RANS model associated with large-scale separated flows [14]. Another possible reason may be due to the large blockage ratio in the experiments at high AOA.

When SB is implemented, the additional momentum carried by the injected fluid accelerates the flow above the upper surface. The

Table 1 Test matrix of case studies

Test model	Volumetric flow rate, lpm	V_∞, m/s	Ma	Re	V_j, m/s	C_μ	α, °
Baseline	0	9.9	0.029	1.35E + 05	N.A.	N.A.	0,4,8,12,14,16,18,20
Streamwise blowing	550	9.9	0.029	1.35E + 05	23.98	0.055	0,8,12,16,20
Streamwise blowing and suction							
Counterstreamwise blowing							
Counterstreamwise blowing and suction							
Suction	550	9.9	0.029	1.35E + 05	0	N.A.	0,8,12,16,20

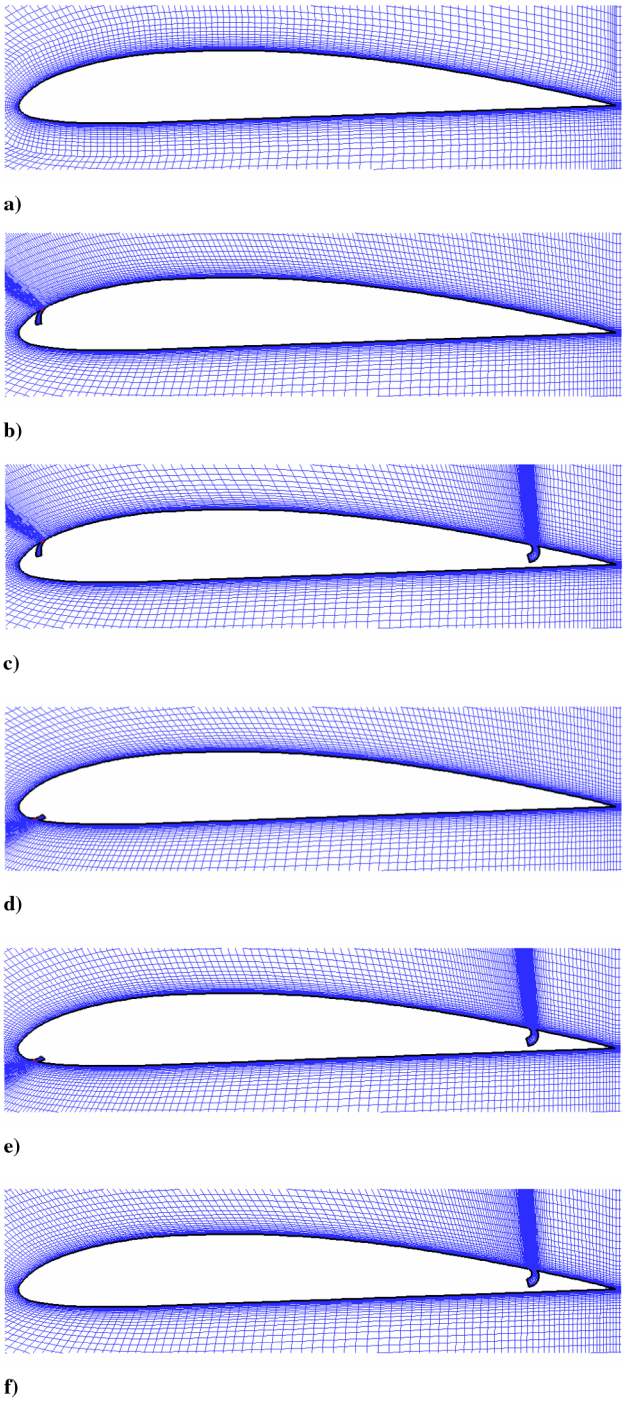

Fig. 2 Meshes for the a) baseline Clark Y airfoil; and modified airfoils with the following configurations: b) SB, c) SB-S, d) CB, e) CB-S, and f) S.

pressure therefore decreases, especially near the injection slot at $X/c = 0.036$ and the stall angle rises to AOA $= 20°$ as seen in Fig. 3e. Good agreement can be found between experimental and numerical results, except at AOA $= 20°$, when flow separation is predicted by the latter. The discrepancy between the computational and experimental results at $X/c = 0.075$ and 0.125 of the lower surface may also be due to the imperfect geometry as described in the earlier paragraph.

For the SB-S (streamwise blowing with suction) configuration, the C_p further decreases along the upper surface, indicative of lift augmentation. However the influence of suction on the reduction in the experimental C_p distribution is limited from $X/c = 0.35$ to 1 for AOA $= 12$ and 16°.

Good agreement between experimental and computational results is found only for AOA $= 0°$ when suction is employed in isolation (S configuration), while moderate agreement can be found for nonzero AOAs. The flow stalls at AOA $= 12°$, unlike the SB and SB-S configurations. In particular, though the positive effects of fluid suction extend over the entire airfoil upper surface in the experiments for AOA $= 8$ and 12°, it is limited from $X/c = 0.3$ to 1 when AOA $= 16$ and 20°. In contrast, the computations predict that fluid suction has a much stronger influence on the C_p distribution for all AOAs. It is possible that some three-dimensional characteristics of suction are not well captured by the 2-D CFD simulations.

The comparisons of C_p distributions for the CB and CB-S cases are not presented, as computational and experimental data reveal different flow characteristics at nonzero AOAs. The computational results predict attached flow for AOAs as high as 16°, while separated flow is observed in the experiments much earlier. Absence of the exact reasons for this distinct disagreement notwithstanding, CB and CB-S are suspected to be highly sensitive to the momentum coefficient, airfoil leading-edge curvature, as well as the injection location and orientation as reported by Wake et al. [12].

B. Comparisons of Aerodynamic Performances and Power Required

As shown in Fig. 4a, the numerical simulations predict the lift force accurately for the baseline model up to AOA $= 16°$. Less drag is predicted than in the experiments, a common observation with RANS model simulations [15], but both sets of data show good agreement in terms of trend. A comparison of CFD results for the lift and the integrated C_p distribution shows that viscous forces have little effect on the lift as shown in Fig. 4a. However, the experimental C_p integral differs by 2.75 to 26.31% with the experimental force measurements for various AOAs. This may be due to the limited number of pressure taps used, especially at the leading edge and the large geometrical blockage ratio at high AOAs. Taking into account the limitation of the experiments as well as the decent agreement of the C_p distribution between the experiments and the simulations, the context that follow (including Figs. 5 and 6) describes only the computational results.

In Fig. 5, the hollow square, circular, and triangular symbols show forces on the airfoil surfaces of the modified airfoils with either flow injection and/or suction, while the corresponding filled symbols with dashed lines represent their coefficients corrected by taking the jet reaction force into consideration, as suggested in [6]. The jet reaction forces in this study are not as significant as those reported by Zha et al. [6] (with jet momentum coefficient of 0.18–0.32), because of the relatively lower jet momentum coefficient (0.055) in this study.

Compared with the baseline, SB not only delays the stall angle from 14 to 16°, but also enhances the lift while reducing drag. When suction is added together with SB, the lift is further enhanced. Although the drag of the airfoil with SB-S is slightly higher than that of SB, it is still less than that of baseline model. Remarkably, thrust is predicted from both the SB-S and SB configurations when AOA$<$ 16°. A comparative analysis between the SB-S, SB, and S configurations (with the baseline as a reference) indicates greater lift augmentation derived from jet injection than suction, in agreement with [10]. The S configuration produces lift enhancement but at the expense of a drop in the stall angle. In addition, the lift enhancement for combined injection and suction is no larger than the sum of individual lift enhancements due to SB and S. This differs from a similar study of a nonconformal CFJ airfoil [9] and may indicate a dependence of the CFJ technique on airfoil geometry.

With the exception of the S configuration, the numerical results predict that all configurations attain an improvement in the stall angle as seen from Table 2. This implies that fluid injection plays an important role in the lateral transport of energy from the jet to the main flow so as to suppress flow separation at high AOAs [10]. While we acknowledge the present disagreement between the experiments and CFD results, it is nevertheless interesting to note the potential performance of counterstreamwise injection relative to its streamwise counterpart especially given the success of Wake et al. [12]. CB achieves a higher maximum lift coefficient (2.03) than that of SB (1.79) at AOA $= 16°$, but is predictably less effective at low AOAs, especially at AOA $= 0°$. The addition of suction (CB-S and SB-S)

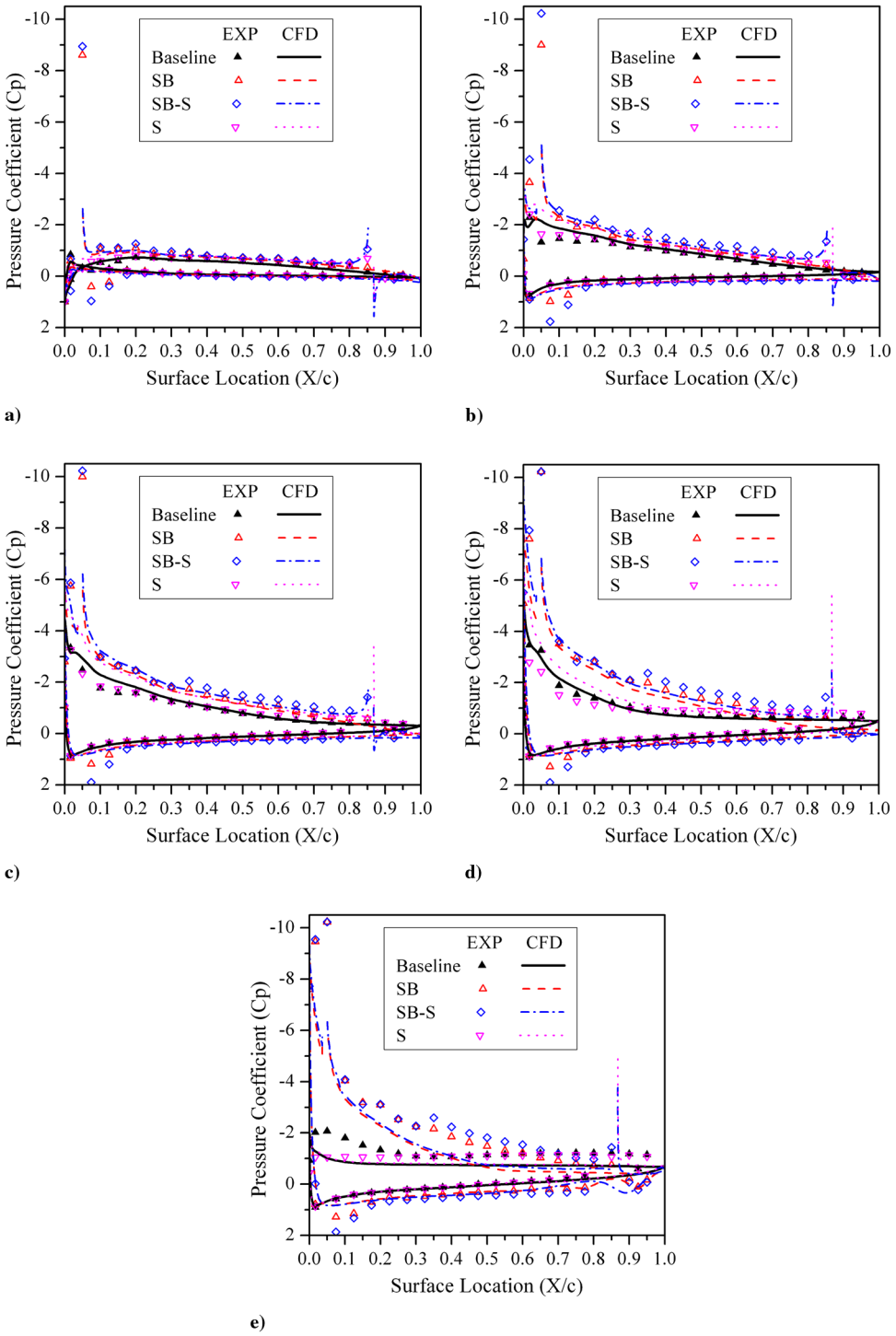

Fig. 3 Comparisons of pressure coefficient distributions for the baseline and modified Clark Y airfoils with SB, SB-S, and S configurations at AOA equals a) 0, b) 8, c) 12, d) 16, and e) 20°.

can further improve the maximum lift coefficient to 2.35 and 2.07, respectively, at AOA = 16°. These corresponding 184 and 162% enhancements in lift over the baseline airfoil clearly place the SB-S and CB-S configurations as the best in terms of overall lift performance. Furthermore, they also achieve significant drag reduction compared with the baseline.

For the same mass flow rate, the power expended by the auxiliary flow is determined mainly by the total pressure ratio (PR) [10]. Figure 6 shows the total pressure ratios of the different cases at various AOAs. For CB and SB, PR is defined as the ratio of the average total pressure at the jet exit to that of the freestream, while for S, it is the ratio between the freestream total pressure and that at the suction inlet. For CB-S and SB-S, the ratio of the total pressures between the injection and suction slots is the adopted definition. The pressure losses within the internal ducts are not considered.

Streamwise injection is found to require less power than counterstreamwise injection (for AOA > 5°) due to the lower static pressure on the upper surface. This effect becomes more pronounced with an increase in AOA due to the gradual decrease in C_p near the streamwise injection slot. There is a slight increase in required power from AOA = 16 to 20° for SB-S due to the incremental power needed for suction. In comparison with injection, the power used for suction is less due to the relatively higher C_p near the suction slot but it increases with the increase of AOA. Finally, systems having both injection and suction (SB-S or CB-S) demand slightly more power than those with only injection (SB or CB).

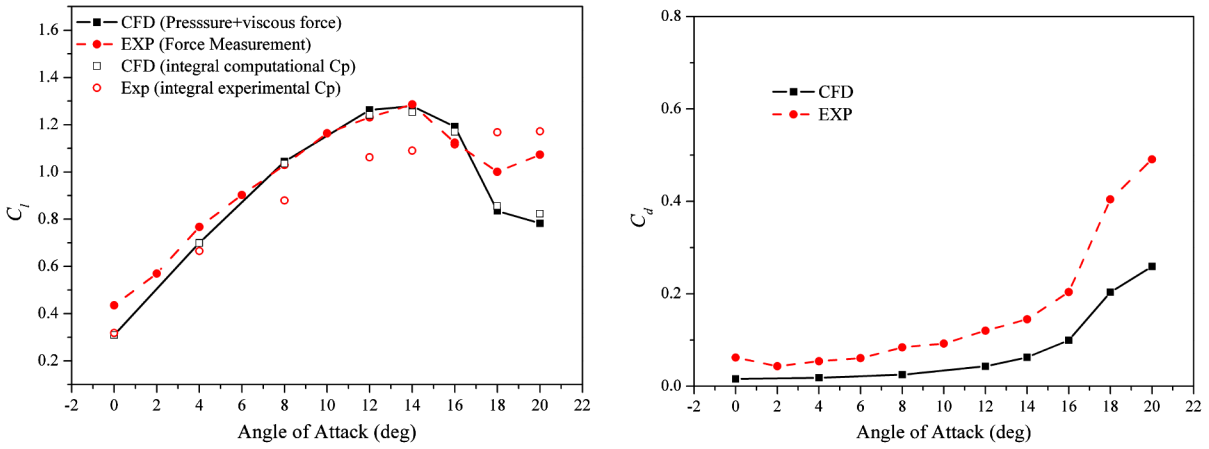

a) b)

Fig. 4 Comparison of the a) lift coefficient C_l and b) drag coefficient C_d for the baseline airfoil.

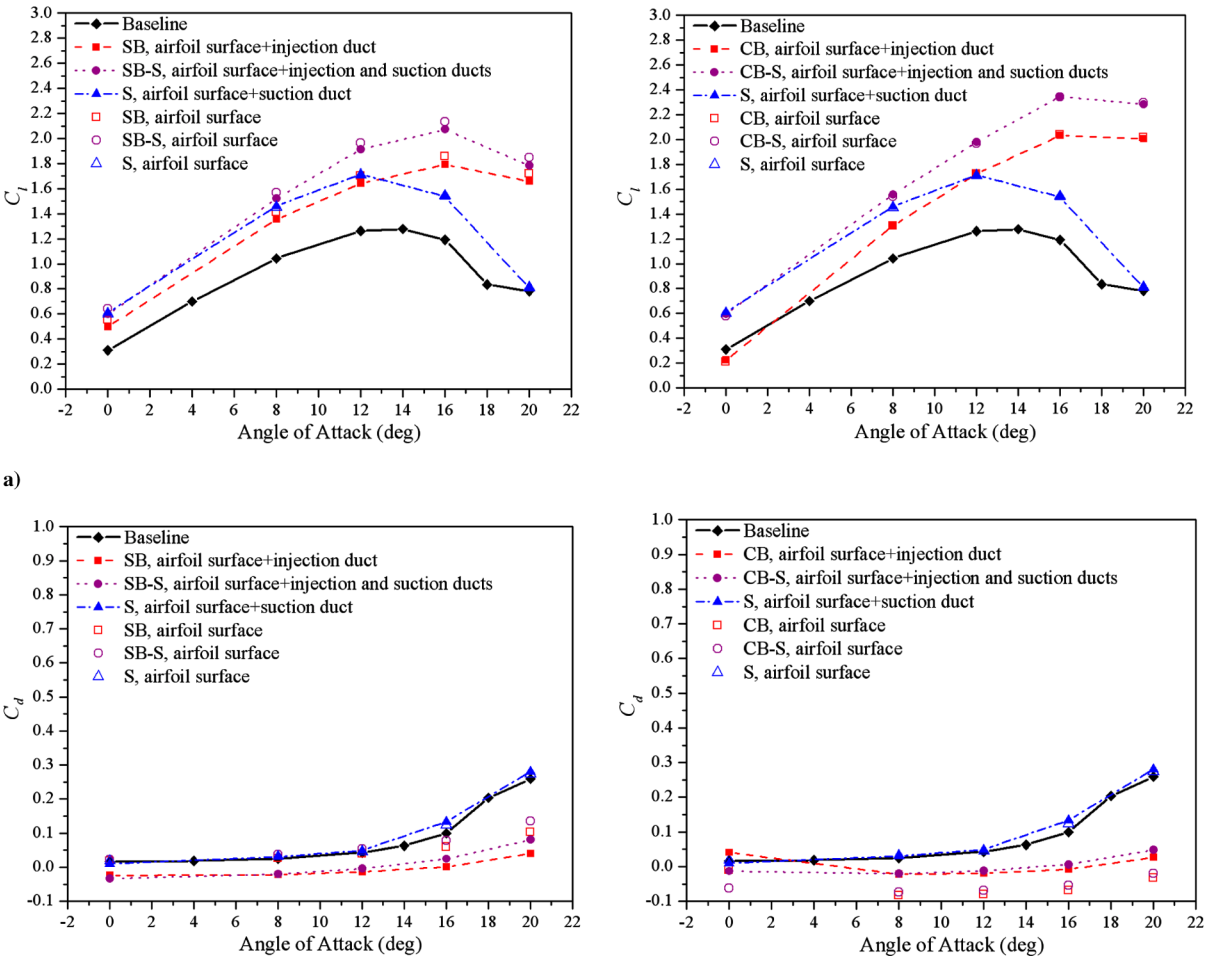

a)

b)

Fig. 5 Computational results of the a) lift coefficient C_l and b) drag coefficient C_d for different combinations of injection and suction.

Table 2 Performance summary of the different combinations of injection and suction

	$AOA_{Cl\,max}$, °	$C_{l\,max}$	$C_{d\,max}$	$C_{d\,min}$	$C_{l\,max}/C_{l\,max_{baseline}}$, %
Baseline	14	1.28	0.26	0.015	
Streamwise blowing	16	1.79	0.04	−0.02448	140
Streamwise blowing and suction	16	2.07	0.08	−0.0336	162
Counterstreamwise blowing	16	2.03	0.03	−0.02245	159
Counterstreamwise blowing and suction	16	2.35	0.05	−0.02101	184
Suction	12	1.71	0.28	0.01012	134

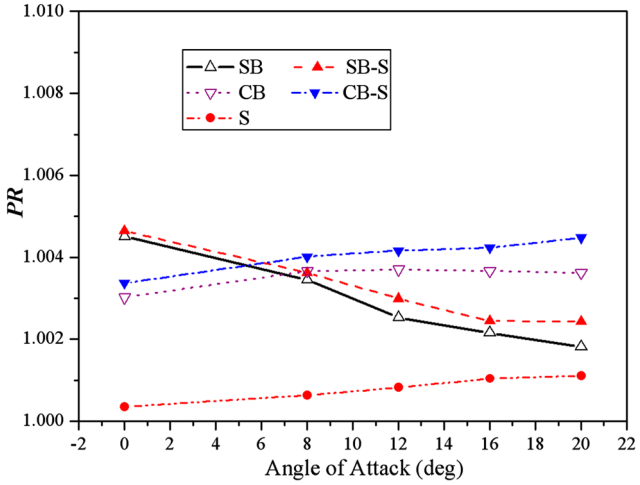

Fig. 6 Computational results of the total pressure ratios for different combinations of injection and suction.

IV. Conclusions

This study demonstrates the success of the conformal CFJ airfoil as an alternative to achieving lift augmentation through suppressing flow separation. Configurations involving combined injection and suction are the most effective, producing increases in lift of up to 184% over the baseline. Compared with suction, fluid injection is a superior tool for increasing lift, though it is stressed that appropriate use of both processes can result in higher operating efficiency. The success of counterstreamwise injection is uncertain, especially given the disagreement between our experimental and computational results and its weaker performance at low AOAs. However, encouraging data from the literature [12], coupled with the fact that our simulations on configurations with counterstreamwise injection predict the largest lift coefficients, are evidence of its potential for future flow control research. Based on the present data, SB-S is found to be the most promising.

The success of the present numerical approach also confirms its value as an efficient design tool for predicting reasonably accurate pressure distributions for 2-D airfoils and active flow control problems involving an introduction of external fluid momentum. Decent agreement between the experimental and computational C_p distributions is generally obtained, with the exception of cases where there is large-scale flow separation.

References

[1] Englar, R. J., "Circulation Control Pneumatic Aerodynamics: Blown Force and Moment Augmentation and Modifications; Past, Present and Future," *Fluids 2000 Conference and Exhibit*, AIAA Paper 2000-2541, June 2000.

[2] Wygnanski, I., "The Variables Affecting the Control Separation by Periodic Excitation," *2nd AIAA Flow Control Conference*, AIAA Paper 2004-2505, June 2004.

[3] Liu, M. Y., Sankar, L. N., Englar, R. J., Ahuja, K. K., and Gaeta, R., "Computational Evaluation of the Steady and Pulsed Jet Effects on the Performance of a Circulation Control Wing Section," *42nd AIAA Aerospace Sciences Meeting and Exhibit*, AIAA Paper 2004-0056, Jan. 2004.

[4] Zha, G. C., Carroll, B. F., Paxton, C. D., Conley, C. A., and Wells, A., "High Performance Airfoil Using Coflow Jet Flow Control," *AIAA Journal*, Vol. 45, No. 8, 2007, pp. 2087–2090. doi:10.2514/1.20926

[5] Zha, G. C., Gao, W., and Paxton, C. D., "Numerical Simulation of Co-Flow Jet Airfoil Flows," *AIAA 44th Aerospace Sciences Meeting and Exhibit Conference*, AIAA Paper 2006-1060, Reno, NV, Jan. 8–12, 2006.

[6] Zha, G. C., Gao, W., and Paxton, C. D., "Jet Effects on Coflow Jet Airfoil Performance," *AIAA Journal*, Vol. 45, No. 6, 2007, pp. 1222–1231. doi:10.2514/1.23995

[7] Zha, G. C., and Paxton, C., "A Novel Airfoil Circulation Augment Flow Control Method Using Co-Flow Jet," *AIAA 2nd Flow Control Conference*, AIAA Paper 2004-2208, June–July 2004.

[8] Zha, G. C., and Gao, W., "Analysis of Jet Effects on Co-Flow Jet Airfoil Performance with Integrated Propulsion System," *AIAA 44th Aerospace Sciences Meeting and Exhibit Conference*, AIAA Paper 2006-0102, Jan. 2006.

[9] Chng, T. L., Rachman, A., Tsai, H. M., and Zha, G.-C., "Flow Control of an Airfoil via Injection and Suction," *Journal of Aircraft*, Vol. 46, No. 1, 2009, pp. 291–300. doi:10.2514/1.38394

[10] Zha, G-C., Paxton, C. D., Conley, C. A., Wells, A., and Carroll, B. F., "Effect of Injection Slot Size on the Performance of Coflow Jet Airfoil," *Journal of Aircraft*, Vol. 43, No. 4, 2006, pp. 987–995. doi:10.2514/1.16999

[11] Chng, T. L., Zhang, J. M., and Tsai, H. M., "A Novel Method of Flow Injection and Suction for Lift Enhancement," *46th AIAA Aerospace Sciences Meeting and Exhibit*, AIAA Paper 2008-335, Jan. 2008.

[12] Wake, B. E., Tillman, G., Ochs, S. S., and Kearney, J. S., "Control of High-Reynolds-Number Turbulent Boundary Layer Separation Using Counter-Flow Fluid Injection," *3rd AIAA Flow Control Conference*, AIAA Paper 2006-3025, June 2006.

[13] Tillman, T. G., and Kistler, A. L., "Scaling of the Bursting Frequency for Turbulent Boundary Layers Approaching Separation," *AIAA Journal*, Vol. 34, No. 5, May 1996, pp. 1070–1072. doi:10.2514/3.13189

[14] Li, D., "Numerical Simulation of Thin Airfoil Stall by Using a Modified DES Approach," *International Journal for Numerical Methods in Fluids*, Vol. 54, No. 3, 2007, pp. 325–332. doi:10.1002/fld.1403

[15] Dam, C. P., "Recent Experience with Different Methods of Drag Prediction," *Progress in Aerospace Sciences*, Vol. 35, No. 8, 1999, pp. 751–798. doi:10.1016/S0376-0421(99)00009-3